

Fourier Transform Infrared Imaging: Theory and Practice

Rohit Bhargava and Ira W. Levin*

Laboratory of Chemical Physics, National Institute of Diabetes and Digestive and Kidney Diseases, National Institutes of Health, Bethesda, Maryland 20892-0510

The signal-to-noise ratio (SNR) of spectral data obtained from a microimaging Fourier transform infrared (FT-IR) spectrometer assembly, employing a step-scan interferometer and focal plane array detector, is analyzed. Based on the methodology of data collection, a theoretical description for the performance characteristics is proposed and quantitative effects of the acquisition parameters on the SNR are explained theoretically and compared to experiment. To obtain the best strategy for achieving either the highest SNR in a given time interval or for attaining a given SNR in the shortest time period, the concept of characteristic plots is introduced. The theoretical analysis is extended to FT-IR microimaging employing continuous scan interferometers in which the advantages of fast image collection are enumerated, while SNR limitations arising from mirror positioning errors are discussed. A step-scan method is suggested for faster data collection in which an optimal detector response and SNR benefits are retained. Theoretically obtained SNRs based upon the expressions proposed in this paper predict experimentally determined values quite well and can be used to obtain an understanding of the required developments for improved performance. Finally, SNRs for both microimaging systems and conventional microspectroscopic instrumentation are compared.

Fourier transform infrared (FT-IR) imaging, employing focal plane array (FPA) detectors, is a relatively new technique for microscopic chemical characterizations.¹ As opposed to conventional FT-IR microspectroscopic instrumentation that employs a single detection element hundreds of micrometers in size,² spectral multiplexing combined with multichannel detection in an FT-IR interferometer, microscope, and FPA assembly enables spectroscopic and spatial discrimination over a sample field of view in minutes.³ To date, FT-IR imaging has been used to examine a variety of polymers and biological systems.^{3–14} Many of these studies were qualitative in nature, since a major requirement for

accurate, sensitive, and rapid analysis, namely, the acquisition of high signal-to-noise ratio (SNR) data in as short a time as possible, was not readily achievable. The first attempts to systematically examine sources of noise and to increase the SNR of collected data were reported more than a year ago¹⁵ in which it was shown that the benefits of an increase in collection time, by increasing the number of frames to be averaged, is limited and that the time-averaging of image cubes is more suited to obtaining high SNR data. Further attempts at obtaining high-fidelity data concentrated on novel collection and postcollection data processing schemes.^{16,17}

The preliminary analysis of noise and SNRs for imaging spectrometers¹⁵ did not explicitly either incorporate the effects of collection parameters or address data collection strategies required for achieving high-fidelity data. It is also unclear which SNR benefits are realized when employing a specific collection/processing strategy due to the lack of theoretical expressions for the SNR incorporating both experimental aspects. Hence, confusion has arisen regarding the capabilities of FT-IR imaging and the choice of the best approach for data collection to yield a desired result. In this paper, we examine the theoretical SNRs achievable by FT-IR imaging by explicitly incorporating instrumental and collection parameters. We then discuss SNRs for different instrumental configurations and demonstrate the formulation of an optimal data collection strategy. Based on an understanding of SNR development as a function of data collection parameters, new approaches to data acquisition and future instrumental developments are suggested.

* Corresponding author: (email) iw@helix.nih.gov; (tel) (301) 496 6844; (fax) (301) 496 0825.

- (1) Colarusso, P.; Kidder, L. H.; Levin, I. W.; Fraser, J. C.; Arens, J. F.; Lewis, E. N. *Appl. Spectrosc.* **1998**, *52*, 106A.
- (2) Bhargava, R.; Wall, B. G.; Koenig, J. L. *Appl. Spectrosc.* **2000**, *54*, 470.
- (3) Lewis, E. N.; Gorbach, A. M.; Marcott, C.; Levin, I. W. *Appl. Spectrosc.* **1996**, *50*, 263.
- (4) Chalmers, J. M.; Everall, N. J.; Hewitson, K.; Chesters, M. A.; Pearson, M.; Grady, A.; Ruzicka, B. *Analyst* **1998**, *123*, 579.

- (5) van der Weert, M.; van't Hof, R.; van der Weerd, J.; Heeren, R. M. A.; Posthuma, G.; Hennink, W. E.; Crommelin, D. J. A. *J. Controlled Release* **2000**, *68*, 31.
- (6) Snively, C. M.; Koenig, J. L. *J. Polym. Sci., Part B: Polym. Phys.* **1999**, *37*, 2353.
- (7) Snively, C. M.; Koenig, J. L. *J. Polym. Sci., Part B: Polym. Phys.* **1999**, *37*, 2261.
- (8) Bhargava, R.; Wang, S.-Q.; Koenig, J. L. *Macromolecules* **1999**, *32*, 2, 2748.
- (9) Bhargava, R.; Wang, S.-Q.; Koenig, J. L. *Appl. Spectrosc.* **1998**, *52*, 323.
- (10) Marcott, C.; Reeder, R. C.; Sweat, J. A.; Panzer, D. D.; Wetzel, D. L. *Vib. Spectrosc.* **1999**, *19*, 123.
- (11) Marcott, C.; Reeder, R. C.; Paschalis, E. P.; Boskey, A. L.; Mendelsohn, R. *Phosphorus Sulfur* **1999**, *146*, 417.
- (12) Mendelsohn, R.; Paschalis, E. P.; Boskey, A. L. *J. Biomed. Opt.* **1999**, *4*, 14.
- (13) Lewis, E. N.; Levin, I. W.; Hanig, J. P.; Lester, D. S. *Biophys. J.* **1996**, *70*, WP180.
- (14) Lewis, E. N.; Kidder, L. H.; Pentchev, P.; Levin, I. W.; Lester, D. S. *Biophys. J.* **1997**, *72*, MPME5.
- (15) Snively, C. M.; Koenig, J. L. *Appl. Spectrosc.* **1999**, *53*, 170.
- (16) Bhargava, R.; Ribar, T.; Koenig, J. L. *Appl. Spectrosc.* **1999**, *53*, 1313.
- (17) Bhargava, R.; Wang, S.-Q.; Koenig, J. L. *Appl. Spectrosc.* **2000**, *54*, 486.

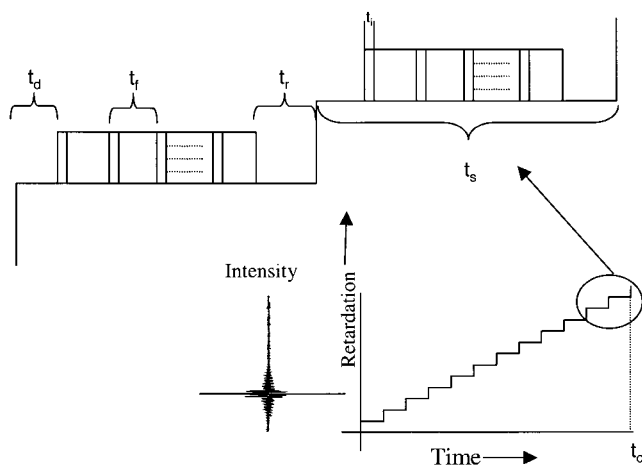


Figure 1. Data collection process for imaging using a step-scan spectrometer and an FPA. The retardation is varied quickly (stepped) and held constant to allow detection and building of the interferogram point by point. For each spectrometer step of time, t_s , there is a time delay, t_d , before collection is initiated to allow the spectrometer to stabilize. A number of frames are coadded at each step, each in time t_f . For each frame, the signal is integrated for a fraction of the frame time, t_i , and all the frames are read, averaged, and stored in time t_c .

Imaging Spectrometers: Overview and SNR Characteristics. An imaging spectrometer typically measures spectra from areas of the order of 1 mm^2 , using thousands of individual detector elements to collect spatially resolved information. This mode differs from the conventional mode of detection in the times required for data collection (due to SNR characteristics), digital signal readout, and storage (due to the large number of detection elements). Detection by the FPA may be carried out either at predetermined time intervals initiated at the start of interferometer scanning (continuously scanning interferometers) or through triggering to collect data at discrete mirror retardations (step-scanning interferometers). Given the generally poor SNR characteristics of FPA detectors for most applications, step-scanning spectrometers have become the preferred choice of instrumentation. We first examine imaging systems utilizing step-scan interferometers as these results can be readily extrapolated toward analyzing systems incorporating continuous-scan interferometers.

In a step-scan interferometer, optical retardation is achieved and maintained for a given time, t_s (Figure 1). The interferometer is then quickly stepped to achieve the next desired retardation, thus building the interferogram by accessing sequential retardations. Since all pixels simultaneously collect data, an image is obtained at each interferometer step for constructing the data set image by image. For each optical retardation of the interferometer, the FPA is triggered to collect data after a time delay, t_d , to allow for spectrometer stabilization. A specific number of frames are averaged in time t_f for each frame and stored in the computer in time t_f to achieve the time-averaged image corresponding to the retardation. The time required to obtain each average frame of data is the sum of the time for detecting and digitizing the signal, for reading the signal to the computer, for temporarily storing the signal, for applying a calibration correction, and finally for averaging the signal and storing the data to the disk. The integration time (t_i), number of frames (n_f), and number of steps (n_s) to construct the interferogram determine the total time that the signal intensity is detected.

For a conventional wide-beam single-element detector in an FT-IR spectrometer incorporating a Michelson interferometer, the SNR achieved in time, t , is represented by¹⁸

$$\text{SNR} = \frac{U_{\bar{\nu}}(T)\Theta\Delta\bar{\nu}\xi}{\text{NEP}}t^{1/2} \quad (1)$$

where, $U_{\bar{\nu}}(T)$ is the spectral energy density at a given wavenumber, $\bar{\nu}$; the noise equivalent power (NEP) is defined by the ratio of the square root of the detector area, A_D , to the measure of its sensitivity, D^* (specific detectivity); Θ is the throughput; $\Delta\bar{\nu}$ the spectral resolution; and ξ is the spectrometer efficiency. This relation is a measure of the ratio of signal to the root-mean-square (rms) noise for single beam spectra. For examining the SNR for FT-IR microspectroscopic measurements, using a single element detector and apertures to delineate areas from which spectra are obtained, a correction, δ , was proposed to (1) yielding the modified equation,¹⁹

$$\text{SNR} = \frac{U_{\bar{\nu}}(T)\Theta\Delta\bar{\nu}\xi}{\text{NEP}}\delta t^{1/2} \quad (2)$$

In extending this concept to a microimaging spectrometer,¹⁵ a relationship for the SNR of a single pixel on the FPA was proposed as

$$\text{SNR} = \frac{0.12\pi A(1 - \sqrt{1 - (\text{NA})^2})U_{\bar{\nu}}(T)\Delta\bar{\nu}D^*}{\sqrt{A_D}}t^{1/2} \quad (3)$$

where NA is the numerical aperture and A the area of the sample imaged onto the pixel. The correction due to apertures is not required and the efficiencies were taken to be commonly encountered values.

EXPERIMENTAL SECTION

A. Instrumentation. The imaging setup used in this study consists of a step-scan spectrometer²⁰ (Bruker IFS-66/s), an infrared microscope equipped with all-reflective Cassegrainian optics (ImageMax, SpectraTech Inc.), and an FPA²¹ (Santa Barbara Focalplane). All experiments are carried out in a transmittance mode using a single BaF_2 disk for sample placement to avoid any sample effects.² A $15\times$ objective is used to image a sample area field of view ($\sim 500 \mu\text{m} \times 500 \mu\text{m}$) onto a 64×64 pixel HgCdTe (MCT) FPA that is equipped with an optimally sized cold shield.²³ A diffuser is placed in the beam path to increase spatial homogeneity, and a band-pass filter is used to restrict the optical bandwidth to that of interest. An additional filter is used for further reducing the intensity when necessary (as with a lower frame rate,

(18) Griffiths, P. R.; de Haseth, J. A. *Fourier Transform Infrared Spectrometry*; Wiley-Interscience: New York, 1986.

(19) Messerschmidt, R. G. In *Infrared Microspectroscopy: Theory and Applications*, Messerschmidt, R. G., Hartcock, M. A., Eds.; Marcel Dekker Inc.: New York, 1988.

(20) Bruker Optics, Billerica, MA.

(21) Santa Barbara Focalplane, Santa Barbara, CA.

(22) Bhargava, R.; Wang, S.-Q.; Koenig, J. L. *Appl. Spectrosc.* **1998**, *52*, 323.

(23) Bhargava, R.; Fernandez, D. C.; Schaeberle, M. D.; Levin, I. W. *Appl. Spectrosc.* **2000**, *54*, 1743.

vide infra). The retardation time of the spectrometer at each step can be varied arbitrarily with a minimum corresponding to the mirror stabilization time (40 ms). The collected FPA signal is determined by the frame rate (315.1, 252.1, and 180.1 Hz, corresponding to integration times of 0.099, 0.124, and 0.1488 ms/frame, respectively) and the number of frames averaged. The array signal is then read to a computer (allowing ~ 100 ms for readout, averaging, and storage) before triggering the next step. The time required for trigger pulses is typically of the order of tens of microseconds, which is negligible in comparison to other times in the collection process.

B. Data Collection and Processing. A total of 512 data points are collected over the mid-infrared region ($0\text{--}3950\text{ cm}^{-1}$) providing 4096 spectra at a nominal resolution of 16 cm^{-1} . Determined primarily by the number of frames collected, collection times were 75 s to 8 min for each data cube. Prior to acquiring data, the focal-plane array is flat-fielded to compensate for variation in individual detector response and nonuniform illumination by a two-scene calibration at minimum and maximum interferogram intensities. A fast Fourier transform using triangular apodization was performed on image interferograms to produce single-beam images. The ratios of two similarly collected images are taken pixel by pixel to obtain absorbance image cubes (100% lines). All processing was carried out on a 750-MHz PC with 384 MB of RAM using computer routines written in-house using IDL/ENVI.²⁴

C. Signal, Noise, and SNR Determinations. Unless specified, all data reported in this paper are based on absorbance noise. Due to unavoidable manufacturing differences, each detector on the FPA is practically unique in its response over the mid-infrared range. The pixel-to-pixel gain uniformity is typically of the order of 6–8%, which is convoluted with the signal nonuniformity determined by microscope optics and diffuser compensation. In addition, especially for lower SNR single-beam spectra, the determination of a local slope to correct for absolute intensity variations before determining signal and noise characteristics is error prone. For a 100% line, the slope is zero at every pixel and the noise is readily calculated. Moreover, absorbance measurements are usually more relevant and offer a rigorous test for quantitative determinations. Results between analyses examining the two types of noise should reflect the same trend, although the absolute magnitude of peak-to-peak noise and its standard deviation is expected to be larger. In an FT-IR imaging configuration, FPA detector noise is greater than all other sources of noise combined. Hence, the examination of detector noise is particularly relevant at this stage of the development of this imaging technique. For general sources of spectrometer/microscope noise and their analyses, excellent studies are available.^{18,19,25}

THEORY, RESULTS AND DISCUSSION

A. Imaging Systems Incorporating Step-Scan Interferometers. (1) Collection Time. The first factor influencing the SNR during the collection process is the time required for data acquisition. The minimum collection time to obtain one interferogram data cube is given by

$$t = n_s [t_d + n_f t_f + t_r] \quad (4)$$

where t_f is the time required to acquire each frame. The collection time depends not only on the number of spectrometer steps (a function of spectral resolution and range), as expected, but also on the camera electronics and number of frames used to obtain the average frame data. The frame rate ($1/t_f$) that is used is often determined by signal and dynamic range considerations. The readout time is primarily determined by system electronics. For optimal data collection, the collection time should be no more than the minimum time specified in eq 4.

While the collection time is the time required to obtain an interferogram, the photon flux detection time (i.e., starting time) is the signal integration time, t_i , which is a fraction of the frame time given by $n_s [n_f t_f]$. Hence, a data acquisition efficiency factor may be introduced that accounts for the fraction of time that data are actually being collected. The expression for the SNR then becomes

$$\text{SNR} = \frac{U_v(T)\Theta\Delta_v}{\text{NEP}} \xi \left[\frac{n_f t_f}{t_d + n_f t_f + t_r} \right]^{1/2} t^{1/2} \quad (5)$$

where ξ incorporates the combined efficiency of the spectrometer, beam diverting optics, and microscope optical elements.

(2) Increasing the SNR through Frame Coaddition. Equation 5 implies that the scaling of the SNR with number of coadded frames for a given experimental time is not a simple one. The effect of changing the number of frames on the SNR is given by an acquisition ratio, ϵ_c , which may be defined as

$$\epsilon_c = \left[\frac{n_f t_f}{t_d + n_f t_f + t_r} \right]^{1/2} \quad (6)$$

The acquisition ratio is presented as a function of coadded frames for some commonly used frame rates in Figure 2. In the limit that very few frames are coadded, the ratio scales as $n_f^{1/2}$; while in the limit that the delay and readout times are small compared to other terms, the ratio will approach a constant value determined by the fraction of frame time used for integration. A power (0.5) law trend is seen in the plot (Figure 2) for the ratio as a function of coadded frames. For large numbers of coadded frames, n_f , or when the sum of the readout and delay times is small, the numerator changes at approximately the same rate as the denominator. Hence, the acquisition ratio, ϵ_c , approaches a constant value determined by the ratio of the integration time to the frame time. The efficiency can never be larger than that dictated by the system electronics, that is, the square root of the ratio of integration time to frame time, which is termed the limiting acquisition ratio. The acquisition ratio is also a measure of the efficiency of the data acquisition protocol and can be used as a stand-alone comparison metric for different protocols.

Expressions 5 and 6 demonstrate that the SNR achieved by conducting “constant measurement time” experiments, where the collection time is held constant and numbers of frames averaged is varied, will depend only on the acquisition ratio. Results of such an experiment were first reported Snively and Koenig,¹⁵ in which for a stepping rate of 1 Hz, a sharp increase in the SNR was

(24) RSI Inc., Boulder, CO.

(25) Manning, C. J.; Griffiths, P. R. *Appl. Spectrosc.* **1997**, *51*, 1092.

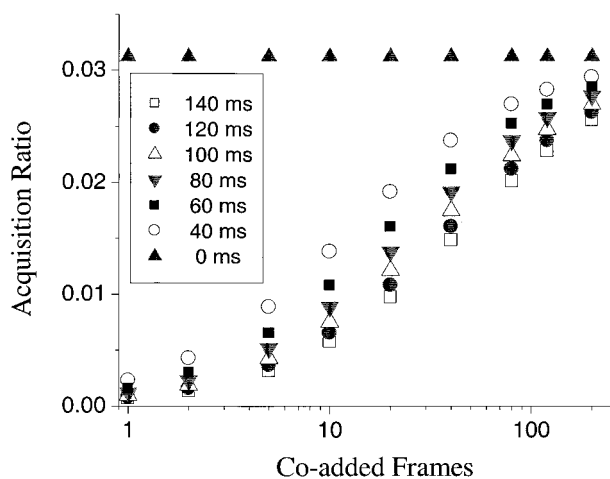


Figure 2. Acquisition ratio as a function of coadded frames for a frame rate of 315.1 Hz as predicted by eq 6 in the text. The ratio varies with the sum of delay and readout times (shown for each data set in the legend) and approaches a limiting value as more frames are coadded. This limiting value, corresponding to the hypothetical case of a zero sum of delay and readout times, is the product of the frame rate and integration time and depends on system electronics.

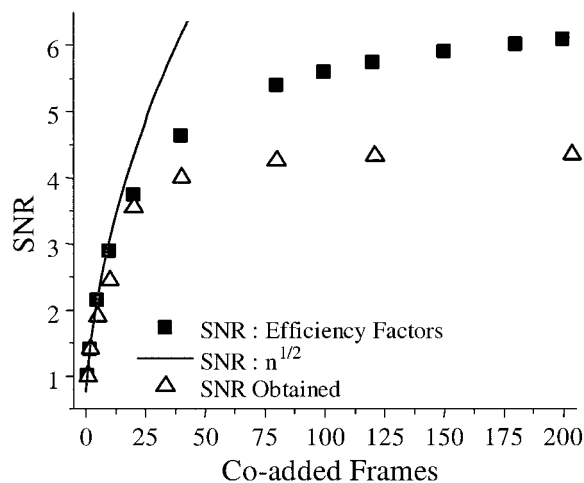


Figure 3. Expected SNR increase as a function of coadded frames compared to the SNR obtained experimentally for a frame rate of 315.1 Hz. If coadding frames were true statistical coaddition, the expected trend would be as shown by the $n^{1/2}$ curve.

observed followed by a plateau in values. We report a similar qualitative trend in our system (Figure 3) in which a normalized SNR using a single-image cube or single-frame data as reference demonstrates a good correlation between experimental and predicted values. In practice, it is inefficient to fix experimental times for all frame rates and numbers of coadded frames. The minimum experiment time, obtained using eq 4, should be employed for data collection. Hence, the total integration time or number of frames will be the only quantity determining the SNR. The theoretically expected trend (as shown in Figure 3 by a solid curve) is extrapolated from the experimental noise level at one frame following a $n^{1/2}$ dependence. It is noteworthy that the SNR values obtained by conducting either a “constant time” experiment or one in which the experiment time varies with numbers of averaged frames are identical. Hence, for experimentally observed SNRs, the expected trend for the optimal experiment time is closely followed when less than ~ 10 frames are coadded.

The deviation from predicted values for coadding more than 20 frames is not a breakdown of the theory, but lies in the nature of the noise in FPAs. Frame coaddition has been thought to be an integration process,¹⁵ and hence, noise does not decrease with the expected square root trend as electrical noise starts to build. However, we do not see the buildup in noise (decreasing SNR) for larger numbers (100, 200, 300) of coadded frames. Noise is marginally lower as the numbers of frames increase and is almost constant once the plateau is achieved. This implies that the cause of the flattening of the noise lies in factors other than the simple buildup of electrical noise with time.

(3) Noise, Dynamic Range, and Frame Coaddition. Noise is intimately related to the number of coadded frames, which tempts the practitioner to decrease the noise as much as possible through frame coaddition. However, the noise must also be sufficient to allow proper signal digitization; that is, the dynamic range of the interferogram must be smaller than the dynamic range of the analog to digital converter (ADC). Further, frame coaddition must be carried out with sufficient computer word length to prevent further digitization errors. Noise arising during interferogram collection can be estimated by examining the dark current of the FPA, which is determined by placing a reflective metal plate in front of the FPA to block all sources of radiation outside the housing. The dependence of noise due to the dark current on the numbers of averaged frames is shown in Figure 4a. A trend similar to that for the decrease in noise observed for 100% lines is observed. Peak-to-peak dark current noise is responsible for systematic baseline variations in wavelength space (the Fourier transform of a spike). Also, small intensity changes in the dark current may lead to changes in the 100% lines. There is also a small amount of thermally excited signal and electrical (probably, storage and read) noise associated with the FPA electronics. Thus, the starting time-dependent noise would decrease until noise from these sources dominates the total noise. It is reasonable to expect that noise attributed to the reading and storing of data would be independent of coadded frames. Hence, a plateau is seen for the SNR when increasing numbers of frames are coadded. A small benefit arises for larger numbers of coadded frames even after the “plateau” and is possibly due to averaged random thermal fluctuations.

To determine whether all noise arises from the dark current of the FPA, the predicted magnitude from dark current analyses is compared to experimentally determined SNRs. While the qualitative behavior of the noise variation is the same as the development of the SNR (Figure 4a), the dark current noise decreases by a factor of ~ 18 , while the SNR only improves by a factor of ~ 4.3 for the same range of coadded frames, as shown in Figure 3. Hence, the dark current is not the sole source of noise. For large numbers of coadded frames, the noise achieves a plateau level of ~ 1 unit. In the same units of measurement, the magnitude of the interferogram at zero interferometer retardation is ~ 7000 units. This implies that the dynamic range of the interferogram is ~ 2 ,¹⁵ as the peak-to-peak noise is ~ 5 times larger than rms noise. If this were the true noise in the interferogram, one would need only to coadd 10 frames (noise level ~ 4 units); otherwise, performance would be degraded by digitization noise. However, digitization noise does not appear to be a problem as the observed noise is greater than this detector noise.

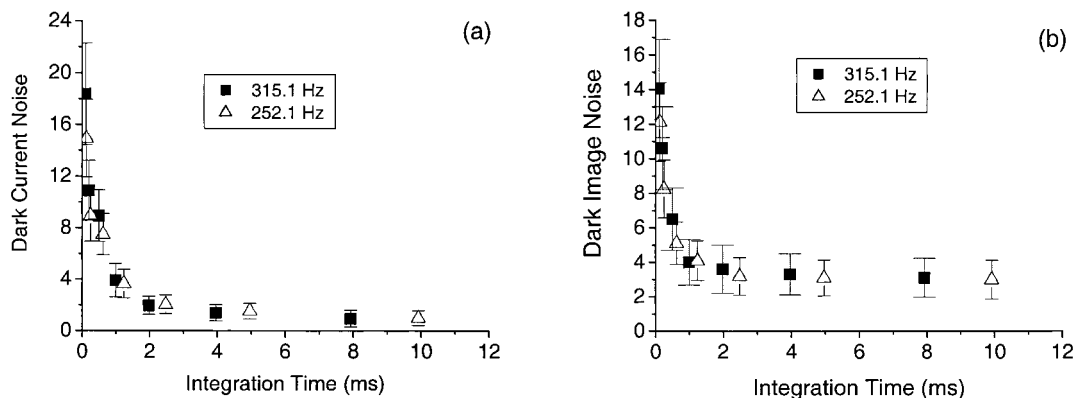


Figure 4. (a) Noise in the dark current of an FPA as a function of the integration time when a metal plate is placed in front of the FPA body. (b) Dark image noise of an FPA as a function of the integration time when a metal plate is placed at the radiation source.

Another approach in examining the FPA output in the absence of spectrometer-modulated radiation is to block the spectrometer source instead of the detector. By eliminating radiation in this manner, the detector senses only emission from the sample and optical components of the instrument. Scintillations due to thermal air currents are also detected. To differentiate dark current noise from these additional noise sources, we use the term “dark image” noise. As expected, the dark image noise is greater than the dark current noise and is shown as a function of coadded frames in Figure 4b. The same trend as the dark current is observed; however, the plateau value is only ~ 4 – 4.5 times smaller than the noise at 1 frame. The noise for both frame rates is also in agreement with previously postulated dependence of noise with increasing integration time. Thus, the qualitative behavior of the dark image noise is very similar to that of the noise actually obtained during an imaging experiment. A plot of the inverse of noise shows the same trend as in Figure 3.

If we consider only the number of frames collected, there are significant advantages to using a lower frame rate for smaller numbers of coadded frames due to the integration time being a constant fraction of the frame time. Hence, if a small number of frames are coadded, it is better to employ a lower frame rate and insert a neutral density filter to reduce the radiation flux. For example, if 1 frame is collected per step, an increase of less than a fraction of a percent in collection time (for 252 vs 315 Hz) will result in $\sim 20\%$ lower dark current noise. For the plateau region, the choice of frame rate does not appear to influence dark current noise. A comparison of this predicted and observed noise with increasing numbers of coadded frames based upon the 100% line data can be seen in Figure 5 for two different frame rates. The fitted line is for the data from the higher frame rate only. Data from the lower frame rate lies above the line (less noise for the same number of frames) as expected. From an analysis of the dynamic range, it can be seen that the ADC is sufficiently sensitive for these noise levels and the interferogram will always be sampled correctly.

(4) Frame Rates. As apparent from the discussion above, a number of frame rates are available for most FPAs, and selection of a specific frame rate is not trivial. For example, a lower frame rate can be used for longer integration times in conjunction with a neutral density filter, and hence, a higher SNR is attained without changing the detector gain. Another benefit of using a neutral density filter is to achieve better spatial homogeneity of the signal.

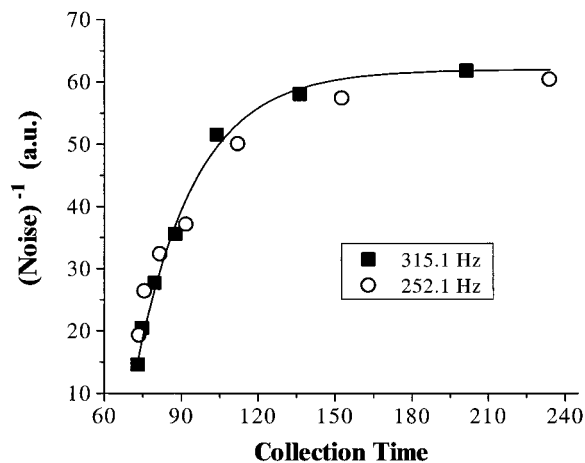


Figure 5. Decrease in noise as reflected in a SNR increase. The fitted line is for the data set collected at 315 Hz only. For a small number of frames, the advantages of collecting at a lower frame rate can be seen.

Changing frame rates is preferable to changing the detector gain to amplify the signal, since altering the detector gain also increases noise in a complex, and not necessarily beneficial, manner.²⁶ A small increase in stray, unmodulated radiation is observed for low frame rates, which is consistent with the higher integration times and may potentially lead to a decrease in the achievable interferogram dynamic range. For a given experimental time period, the number of frames averaged decreases for a decrease in frame rate. For the results being discussed, changing the frame rate does not change the efficiency of data collection because of the constant ratio of starting time to frame time set by the manufacturer for all frame rates. This ratio ($1/32$ of the frame time) depends critically on the FPA electronics, spectral range sensitivity, and ambient temperature. While we have discussed this constant-ratio case above, there are FPAs whose integration time for a specified frame rate may be changed. The analysis outlined above may be used to calculate new characteristics for comparison when the integration time is changed (vide infra) for comparisons between different sets of frame rates and corresponding integration times.

(5) Image Coaddition. It has been demonstrated that time averaging of image cubes results in an increase of a spectral SNR

(26) Bhargava, R.; Fernandez, D. C.; Schaeberle, M. D.; Levin, I. W. *Appl. Spectrosc.* In press.

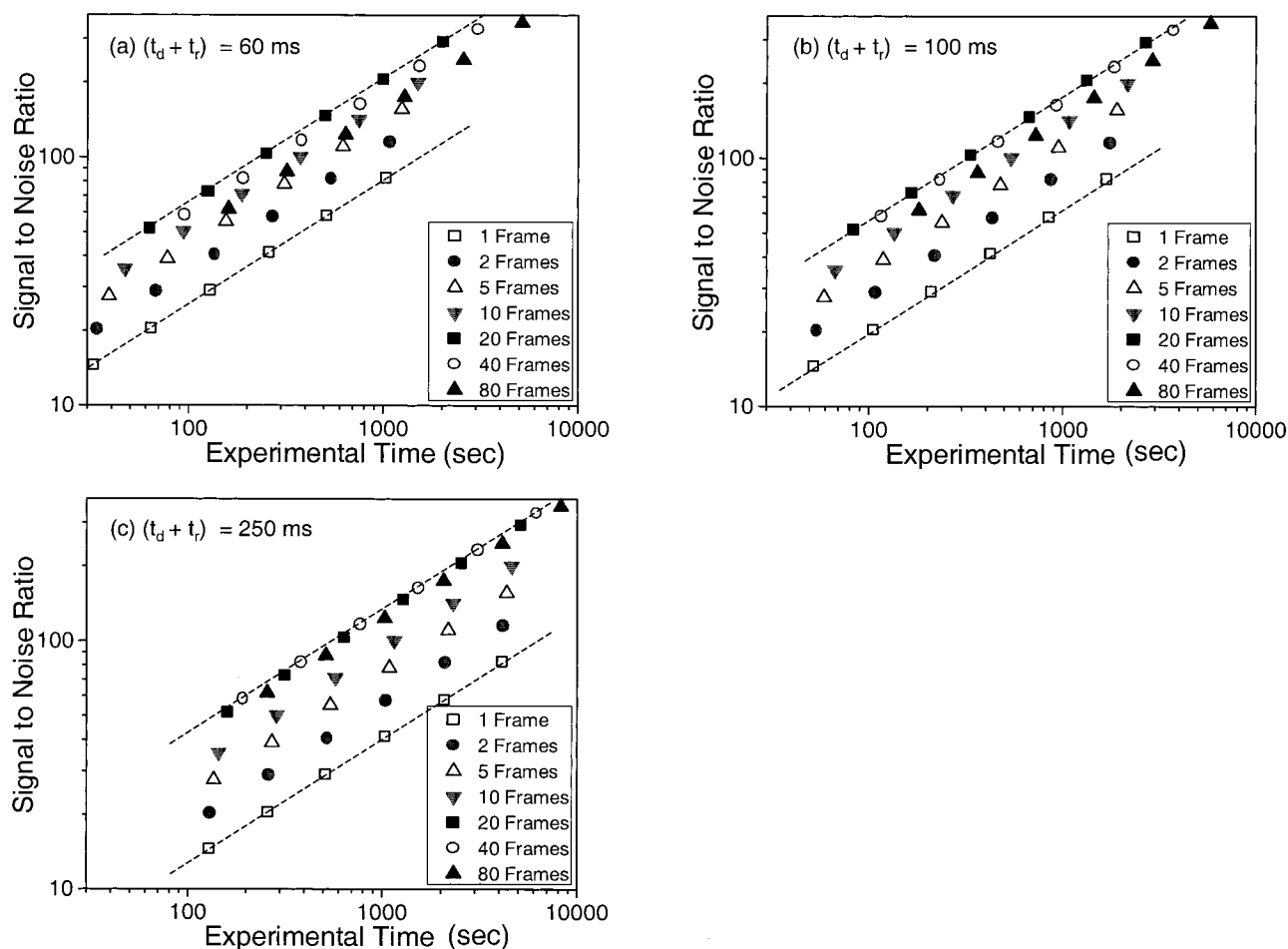


Figure 6. Variation of SNR with increasing readout and storage time per step. (a) For a short total time of 60 ms, collecting 20 frames is optimal, (b) for moderate times, averaging 20 or 40 frames appears to be optimal, while (c) for a large time, the time benefits of coadding 20, 40, and 80 images are similar.

similar to that for time averaging single-element spectra.¹⁵ Hence, the numbers of coadded data sets, n_i , are incorporated into eq 5 as

$$\text{SNR} = \frac{U_{\bar{\nu}}(T)\Theta\Delta_{\bar{\nu}}\xi}{\text{NEP}} \left[\frac{n_i t_i}{t_d + n_i t_i + t_r} \right]^{1/2} (n_i t)^{1/2} \quad (7)$$

where t is the collection time for one image cube. Thus, the expression explicitly incorporates the effect of time averaging data cubes.

(6) Hybrid Collection Strategies and the Determination of Characteristic Plots. The two different collection strategies that yield high SNR data, namely, frame coaddition and image coaddition, may be combined to achieve a net higher SNR than that by simply using one or the other method. In theory, if there is unlimited time available to obtain data, the SNR determined by instrumental limitations (stability and data capacity considerations) may be obtained. In practice, the time available for an experiment is limited, while one desires the highest possible SNR. Conversely, a desired SNR may be required for obtaining in the shortest possible time. Hence, a plot of SNR achievable against experimental time for different collection strategies would be useful. We examine the increase in the SNR arising from a combination of frame and image coaddition only, as the effects of postcollection operations²⁷ on SNR depend on the quality of collected data.

As a general rule, frames are coadded until the plateau in SNR values is achieved and then images are coadded for increased SNR. However, image coaddition is quantized in terms of time; that is, the total collection time is an integral factor of the collection time for a single image. For a desired collection time, there may not be sufficient time to coadd images or there may be enough time to coadd a lesser number of images collected at higher frame rates. A determination of the best collection strategy can be accomplished by an analysis of the SNR obtained for each condition as a function of collection time. These plots may be termed characteristic plots and are shown in Figure 6. The data point with the lowest SNR for each frame rate is the SNR for a single-image data set as determined by experiment. The subsequent data points (slope of 0.5 on a log–log scale) correspond to increasing number of frame coadditions. From the figure, it can be seen that it is almost never beneficial to coadd more than 40 frames. At any given time, it is always more beneficial to coadd $(n + 1)$ images collected by averaging 20 frames at each retardation step than to coadd n images collected by averaging 80 frames. An additional advantage of coadding a larger number of images is to decrease the effect of random noise and drifting of the instrument about the mean. The range of SNR available under the collection conditions is between the dotted lines seen

(27) Bhargava, R.; Wang, S.-Q.; Koenig, J. L. *Appl. Spectrosc.* **2000**, *54*, 1690.

on the figure. coadding images collected by averaging 20 or 40 frames at each optical retardation step is optimal for any given time. By constructing this performance characteristic plot, the optimal collection strategy for a specific experimental protocol may be easily deduced, simplifying parameter selection for the design of experiments.

This analysis does not take into account any computation time for processing images, which may substantially contribute to the total experimental time. This is especially relevant as larger FPAs become available soon. Computational time is nearly independent of the number of frames coadded, although for image coaddition, substantial time may be required for processing and managing multiple data sets. Thus, as the number of coadded images increases, the SNR increases as the square root of number of images, while the collection and computational times increase linearly. If the total experiment is regarded as the sum of the collection and processing times, the characteristic plots in Figure 6 may be modified to yield SNR characteristics for a total experimental time. The incorporation of processing time into the analysis shifts the dotted lines shown by a constant factor to lower ordinate values in the log–log plot. This affects the optimal number of frames required for coaddition and increases the time interval in which a specific SNR may be obtained. As is to be expected, it becomes more efficient to coadd more frames when the processing time per image is larger.

(7) Spectral Resolution. The choice of specific experimental conditions for a required spectral resolution has a complex effect on the achievable SNR. For conventional spectrometers, in which measurement times and optical throughput remain constant, an increase in the spectral resolution by a factor of k results in degradation of the SNR by a factor of k . For imaging spectrometers, the acquisition efficiency is substantially smaller than 1 and is nonlinear with an increase in number of coadded frames. Thus, it may be difficult to improve the SNR for higher spectral resolution data by frame coaddition alone. Further, since the relative SNR characteristics of an FPA, with respect to frame coaddition, are independent of the number of retardation steps, it is not prudent to change the number of coadded frames. That is, only image coaddition should be employed in increasing/decreasing the SNR when decreasing/increasing the spectral resolution. The classical relations between measurement time and spectral resolution are recovered when image cubes are coadded and the processing time is neglected. If the processing time is accounted for in the analysis, the characteristic plots become complex, as the processing time is also resolution (spectral elements) dependent. However, performance characteristic plots for specific cases can be readily made and compared for different resolutions on a case-by-case basis by following the methods discussed in this paper.

B. Imaging Systems Incorporating Continuous-Scan Interferometers. The use of continuous-scan interferometers instead of step-scan interferometers as sources of modulated radiation in a microimaging setup has been demonstrated.²⁸ These authors suggest that the rapid-scanning approach results in a greater SNR in a given time due to the faster collection process facilitated by better electronics. The first difference between the

step-scan and continuous-scan imaging lies in the triggering of the FPA. Data acquisition is initiated at the start of the scan, and interferogram data points are collected at specified time intervals. Hence, the delay time is zero. Compared to a step-scan interferometer run under identical conditions, a continuous-scan interferometer will yield higher SNR data in the same time due to an increased efficiency factor (ϵ_c) given by

$$\epsilon_c = \left[\frac{n_f t_f}{n_f t_f + t_c} \right]^{1/2} \quad (8)$$

which approaches the limiting value of $(t_f/t_c + t_c)^{1/2}$ for 1 frame and $\sim (t_f/t_c)^{1/2}$ for a large number of frames. Compared to step-scan data collection, the efficiency factor is higher for any given frame rate below the limiting efficiency determined by the electronics. It may be concluded that rapid-scan imaging will always be at least as fast as step-scan imaging and, for a specified experimental time, has the potential for higher SNR based on FPA parameters alone. However, the SNR obtainable may be limited by the interferometer characteristics and not the FPA.

(1) Positioning Errors. Rapid-scan imaging has a major limitation in that spectral multiplexing is coupled to the time domain. Hence, there is an error in mirror positioning that corresponds to mirror travel distance, l , over the time for the number of frames coadded. This error in position, Δl , is given by

$$\Delta l = v n_f t_f \quad (9)$$

where v is the scanning velocity. This error may be minimized by collecting only one frame corresponding to every predetermined mirror position, due to which the integration time, and not the frame time, determines the positioning error. In that case, the minimum positioning error is given by

$$\Delta l = v t_f \quad (10)$$

It was suggested that only one frame needs to be measured for fast collection,²⁸ which also minimizes positional inaccuracy. Referring back to Figure 7, we see that coadding images acquired by collecting a single frame per resolution element is far less efficient than coadding a fewer number of images acquired by averaging an optimal number of frames for the same collection time, provided that other parameters are equivalent. In the case where the usual readout and storage times are assumed, when one frame is collected, the continuous-scan imaging spectrometer operates at the lowest FPA efficiency possible. Even when superior electronics are used to lower readout times²⁸ compared to the array reported in this paper, the capture of one frame is of lower efficiency than that obtained by the collection of an optimal number of frames. It may be argued that the storage time for one frame does not involve coaddition and is smaller than the coaddition and storage times required for many frames, as would be the case for step-scan measurements. However, that advantage is more than offset by the requirement to store one-frame image sets and the necessity to access and coadd these sets and then to store the average data set. For sufficient intensity to use a relatively high frame rate (315.1 Hz) to minimize positional errors at a low

(28) Snively, C. M.; Katzenberger, S.; Oskarsdottir, G.; Lauterbach, J. *Opt. Lett.* **1999**, *24*, 1841.

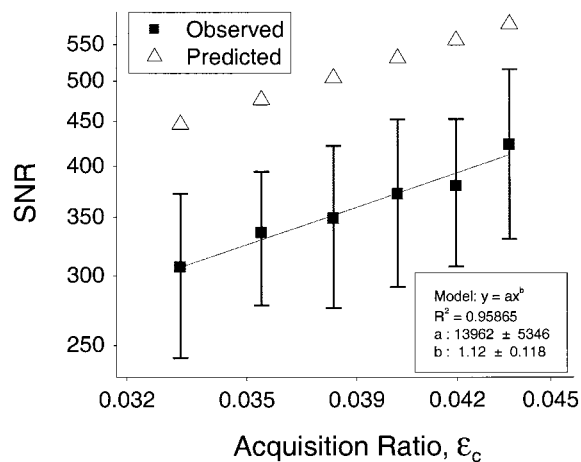


Figure 7. Observed and predicted rms SNR for a 256×256 element MCT detector. The data were acquired by averaging 20 frames at a frame rate of 114.89 using different integration times (0.0255, 0.029, 0.0325, 0.036, 0.0395, and 0.043 ms). The curve fitted to the data is of the form $\text{SNR} = a\epsilon_c^b$, following the expected linear scaling of SNR with ϵ_c .

mirror speed (0.0158 cm/s), ~ 15 nm error in mirror position arises for an integration time of 0.099 ms.

Although the positioning error in continuous-scanning interferometers compares poorly to research-grade step-scan spectrometers in which positioning errors are usually less than 1 nm, performance degradation in an imaging modality may not arise in practice. For the effects of mirror positioning error to be negligible, the positioning error must be small enough to provide a limiting SNR substantially higher than that achievable by the FPA. The SNR due to an error in mirror positioning, Δl , is given by¹⁸

$$\text{SNR}_{\max} = 4/\Delta l \bar{\nu}_{\max} \quad (11)$$

It can be seen that a typical limiting SNR over the mid-infrared region will be greater than 600 for a positioning error of 15 nm. For step-scan measurements, the limiting SNR determined by errors in mirror positioning is greater than 10 000, which is much higher than the SNR (< 500) usually achieved. Hence, the SNR for step-scan imaging spectrometers is primarily due to noise from the FPA and is not dominated by mirror positioning errors. However, the SNR achievable by the FPA and the limiting SNR allowed due to interferometer mirror positioning errors are comparable for rapid-scanning spectrometers, leading to a higher total noise compared to step-scanning instruments. To circumvent this problem, the spectral range collected, the mirror velocity, or the FPA integration time may be decreased. For a given experiment and hardware, it is most expedient to adjust the scanning velocity.

(2) Effect of Changing Mirror Speed. Ideally, the mirror speed for rapid-scan imaging spectrometers must be high enough to modulate the longest detectable wavelength detected at Fourier frequencies (f) within the audio range for easy amplification and filtering and the mirror speed must be small enough to allow sampling of the interferogram at the Nyquist frequency. For example, using the parameters discussed in the previous section, Fourier frequencies ($f_{400} = 12.6$ Hz; $f_{4000} = 126$ Hz) are in the audio

range in the mid-infrared and can be easily amplified and filtered. This implies that the minimum time between two sampling points in the collection scheme must allow for the data to be collected and read from the array. Hence,

$$2\bar{\nu}_{\min} \geq f_{\min} \quad (12)$$

and,

$$4\bar{\nu}_{\max} \leq \frac{1}{[n_f t_f + t_r]} \quad (13)$$

where $\bar{\nu}_{\min}$ and $\bar{\nu}_{\max}$ are the desired lower and higher spectral bandwidth cutoffs, respectively. eq 14 implies that the velocity must be large enough to allow its product with the lowest measured wavenumber to be greater than half the lowest frequency in the audible range (~ 10 Hz). Equation 14 implies that the data collection rate is determined by the detector response, readout, and storage (incorporating an ADC response), in contrast to the digitization rate of the ADC for conventional single-element detector systems. The readout rate of the array, and not the mirror positioning errors, may determine the mirror velocity and, hence, limit the SNR achievable for a given experiment. The readout rate plus a single-frame time becomes the minimum time separation between successive samplings of the interferogram.

To compare with the FPA used in this paper, this minimum time between sampling points is ~ 100 ms at a frame rate of 315.1 Hz. Thus, the minimum time required to collect data (as per conditions used in the step-scan experiments) is ~ 50 s, which is lower than that obtained under identical circumstances using step-scan measurements. However, the SNR resulting from collecting a single frame will be poor (~ 15 assuming validity of step-scan results for the continuous-scan experiment). Using a step-scan configuration and coadding 10 frames, the collection time will be ~ 90 s but the achievable SNR is ~ 35 . To achieve this ratio by rapid scanning and coadding images, the collection time would be ~ 250 s. Hence, for high temporal resolution in a series of images inaccessible by conventional step-scanning interferometers, continuous scanning is a solution. If the temporal resolution is accessible using step-scanning instrumentation at the optimal number of frame coadds, step scanning is the method of choice. In a situation where either hardware improvements or an improved scheme of transferring data digitized by the ADC to computer storage allows for decreased dead time, continuous-scan imaging will become a more attractive tool for high SNR imaging.

From Figure 6, it may be seen that for data collected by averaging one frame per interferogram data point, at least 10 image sets must be coadded to achieve the same SNR as would be obtained from a data set averaging 20 frames per interferogram data point. Hence, in terms of the SNR of data collected, if fast imaging using continuous-scan interferometers is to be comparable to step-scan-based systems, the data acquisition efficiency ratio must be at least 5 times higher for the continuous-scan system. Further, if computation time required for coadding the larger number of data sets is considered, the efficiency of data collection for continuous-scan instruments would need to be even

higher. With current technology, this requirement is rarely met. An imaging mode employing continuous-scan spectrometers will benefit most from improved detector sensitivity and faster electronics.

(3) SNR Limits Imposed by the Interferometer. Some experimental limitations may be placed on continuously scanning imaging spectrometers in terms of operational parameters due to spectral multiplexing in the time domain. Combining eqs 13 and 14, we obtain limits on the mirror velocity:

$$\frac{1}{4\bar{v}_{\max}[n_t t_f + t_r]} \geq v \quad (14a)$$

and

$$v \geq f_{\min}/2\bar{v}_{\min} \quad (14b)$$

If condition 15 is not met by the hardware, rapid-scan detection using an FPA is not possible without modifications. This equation provides a convenient method for determining collection parameters and for checking whether the desired SNR will be obtained before beginning the experiment. Combining eqs 10 and 12–14, one obtains a relation for the achievable SNR (assuming a noise-free detector),

$$16 \left[1 + \frac{t_r}{n_t t_f} \right] \leq \text{SNR} \quad (15a)$$

and

$$\text{SNR} \leq \left(\frac{8}{n_t t_f f_{\min}} \right) \left(\frac{\bar{v}_{\min}}{\bar{v}_{\max}} \right) \quad (15b)$$

These equations are diametrically opposite to the requirements needed for optimal data collection by an FPA. Equations 16a and 16b predict an increase in the SNR by decreasing the time used to collect data relative to the time required to read out the data. From interferometer considerations, the smaller the time expended in collecting data relative to the sampling rate, the less the error due to positional inaccuracies. Also, (16b) implies that the narrower the spectral range used and the smaller the product of the measurement time and the Fourier frequency (i.e., velocity), the larger the achievable SNR.

Hence, a criterion may be established for conducting optimally designed experiments using a continuous-scan imaging spectrometer: the number of frames, frame time, and spectral range are determined primarily by the detector and experimental requirements. Equation 16 should be used to verify whether the SNR predicted by spectrometer performance under those variables is at least 4–5 times greater than that predicted for the FPA. Otherwise, the mirror speed should be changed to achieve that condition. Once the spectrometer operation is as desired, SNR considerations for an imaging spectrometer using a continuous-scan interferometer are exactly those for a continuous-scan single-element detector.

C. Staggered Step-Scan Imaging. Based on the analysis of SNR for imaging spectrometers, a new data collection technique

may be suggested: A step-scan spectrometer is coupled to the standard microscope–FPA assembly. The scan is initiated by the leading edge of an external pulse, whose trailing edge will also trigger data collection by the FPA. The spectrometer is then triggered for a change in retardation by its internal trigger. The FPA is read in a timed sequence of frames. The main advantage of this approach is that it decouples the spectrometer operation from the FPA data collection at each step. Instead, the data collection clocks of the two components are synchronized, and each component's function is independently accomplished by collapsing the delay and read times into a single block where both events occur simultaneously. Utilization of a timed sequence for data collection by the array retains the trigger-free advantages of fast data collection enabled by rapid-scanning interferometry. The implementation of this staggered step-scan idea is demonstrated elsewhere.²⁹

D. Spatial Homogeneity. For a conventional spectrometer that operates with a given detector of a given area, optimal performance is achieved when the detection area is equivalent to the cross section of the beam passing through the interferometer at the maximum allowed solid angle. However, for a microimaging spectrometer, the radiation beam is usually not limited by foreoptics, since the requirement for throughput matching is not as important as the need for signal uniformity over the field of view of the sample. Since the radiation beam has a high-intensity central core that decreases radially outward, the microscope optics are aligned to match the core to the center of the array. Since, the image of the cross section of the output beam from the spectrometer is projected onto the FPA, the signal at any pixel is a convolution of its spatial location on the array and the intensity profile of the cross section of the radiation beam.

Often, incident spectral energy density is sufficient to saturate the ADC of at least some of the individual detector elements, an unacceptable condition for quantitative spectroscopic measurements. Hence, the maximum available spectral density (“signal”) is determined by the available dynamic range, which may be decreased by a component emanating from components of the microscope. Although, the FPA optics and the electronics may also influence spatial homogeneity, these are not critical to most imaging applications. They result, however, in reduced SNR and may offer wavelength-dependent variations. For a given wavelength, taking the ratio to an appropriate background usually results in a high-fidelity image provided that noise variation is not temporal in nature. An expression has been proposed in terms of a correlation coefficient, ρ , to determine whether the noise is predominantly spatial or temporal:

$$\rho = \frac{\frac{1}{S} \sum_{i=1}^S x_{it} x_{it} - \left[\frac{1}{S} \sum_{i=1}^S x_{it} \right] \left[\frac{1}{S} \sum_{i=1}^S x_{it} \right]}{\frac{1}{S} \sum_{i=1}^S x_{it} x_{it} - \left[\frac{1}{S} \sum_{i=1}^S x_{it} \right]^2} \quad (16)$$

where S is the total number of detection elements, x_{it} is the intensity of pixel i at time t , and τ indicates some fixed time relative

(29) Bhargava, R.; Fernandez, D. C.; Schaeberle, M. D.; Levin, I. W. *Appl. Spectrosc.* **2001**, *55*, 1079.

to t . A correlation coefficient, ρ , close to 1 implies that noise is primarily spatial. It has been reported that this is indeed the case for starting MCT FPAs used for imaging.¹⁵

In some cases, this spatial noise may create complications when the ratio of two images is taken. Pixel-to-pixel variations give rise to spatial (or fixed pattern) nonuniformity, which may be corrected by electronic compensation at different intensity levels. The camera is usually calibrated at two intensities to correct pixel-to-pixel nonuniformities. Nonlinearities in detector response, which may be significant over the large response range involved in collecting interferograms, may render the nonuniformity correction ineffective and lead to a residual fixed pattern noise. Although, the use of absorbance images can substantially reduce these "static" noise sources, pixel, array, and system $1/f$ noise cause a drifting component in the spatial noise. The introduction of a sample in the beam path, as well as changes in operating environment and radiation intensity levels, may lead to errors convoluted by the "corrective" action of the calibration. Until corrections are implemented, spatial noise continues to be a limiting noise factor.

E. SNR for a Microimaging Spectrometer. The expression for the SNR of a single pixel on an FPA in an imaging spectrometer is proposed to be

$$\text{SNR}_{\text{FPA}} = \frac{2\pi AU_{\nu}(T)(1 - \sqrt{1 - (\text{NA})^2})\Delta_{\nu}\xi\delta_{\text{FPA}}\epsilon_c(n_1 t)^{1/2}}{\sqrt{A_{\text{D}}/D^*}} \quad (17)$$

The throughput has been expressed in terms of the sample area imaged (A) and the numerical aperture (NA).³⁰ The spectral energy density for a commonly used globar source operating at ~ 1200 K, $U_{2000}(1200)$, is calculated to be 0.87×10^{-3} W/(sr cm² cm⁻¹). For a small-format MCT detector (using $61 \mu\text{m} \times 61 \mu\text{m}$ pixels and a $D^* \sim 3 \times 10^{10}$ cm Hz^{1/2} W⁻¹) acquiring data from a $500 \mu\text{m} \times 500 \mu\text{m}$ field of view, the sample area imaged is 6.1×10^{-7} cm². The numerical aperture for the $15\times$ objective is 0.58. Commonly encountered spectral resolution and acquisition ratio values of 16 cm⁻¹ and 0.01, respectively, are assumed. The spectrometer efficiency is usually taken to be 0.1. The efficiency of the microscope is taken to be 0.6 to account for additional mirrors required to divert light and for reduced transmission through neutral density (diffuser) and band-pass filters. Hence, the theoretically predicted value of rms SNR for a single pixel obtained by collecting one image data cube ($n_1 = 1$) in 105 s is ~ 3100 . The corresponding peak-to-peak SNR predicted is ~ 600 . The experimentally observed peak-to-peak SNR of a single pixel for the same parameters is ~ 110 , which is smaller than predicted.

The predicted and experimentally observed SNR for a 256×256 MCT ($30 \mu\text{m} \times 30 \mu\text{m}$ pixels) imaging a $750 \mu\text{m} \times 750 \mu\text{m}$ area using the same interferometer–microscope assembly as above are shown in Figure 7. The frame rate of the detector was kept constant, and the integration times changed. The observed SNRs are in excellent agreement ($\sim 70\%$) with predicted values. In the theoretical analysis, we have not accounted for additional

noise due to detector architecture, as for example, spatial variation of signal, noisier charge transfer due to the hybrid nature of the array, pixel cross-talk, current leakage, and higher readout noise due to smaller addressing circuits. This may partially explain the difference seen between the theoretically predicted and experimentally observed SNR. Given the assumptions of efficiency and detector response, the agreement between the proposed theory and observed values is quite good.

F. A Comparison of Microspectroscopic Techniques. It is interesting to compare the theoretical performance of a single pixel from the FPA with that of a single-element microscope–spectrometer measuring signal from nearly the same area ($10 \mu\text{m} \times 10 \mu\text{m}$). If we assume that the same interferometer is used to supply the modulated radiation and that the total collection time is the same, then the relative SNR can be compared reasonably by the ratio

$$\frac{\text{SNR}_{\text{FPA}}}{\text{SNR}_{1\text{-element}}} = \frac{\delta_{\text{FPA}}\epsilon_c\text{NEP}}{\delta_1(\sqrt{A_{\text{D}}/D^*})} \quad (18)$$

where δ_1 is the efficiency for the single-element microscope incorporating reflecting mirrors and the aperture and NEP is the noise equivalent power of the single-element detector. The acquisition efficiency was assumed to be 0.03 for an FPA collecting data at 315 Hz. For the single-element microscope assembly, assuming an efficiency due to diffraction of 0.5¹⁹ (a $10\text{-}\mu\text{m}$ specimen is 1 wavelength wide at 1000 cm^{-1} , the lower end of the mid-IR spectral region) and an additional efficiency factor of 0.6 due to mirrors, the overall setup efficiency (δ_1) is 0.3. A typical NEP value for a single-element $0.25 \text{ mm} \times 0.25 \text{ mm}$ square MCT detector¹⁹ (5.5×10^{-13}) is used. The resultant ratio of 0.25 implies that the achievable SNR of a single FPA pixel is actually smaller than that of a spectrum obtained from a single-element detector. Since some of our assumptions favor the single-element detector spectrometer (e.g., a spatial resolution of $6 \mu\text{m}$, typical for imaging systems, would favor the FPA system), a reasonable conclusion is that the SNR obtained from a single FPA pixel is the same as would be obtained by a single-element detector.

The primary reason for this equality is the very low acquisition ratio of FPA-based systems. If the ratio could be raised even to a modest 10% from its current $\sim 1\%$ value, then the FPA-based systems would have significant SNR advantages even for single-point measurements. In practice, the effects of mapping/imaging a large area, spatial resolution, nonequal throughputs, and stage movement time all need to be considered when discussing advantages for mapping measurements over large sample areas. In comparing collection times of an FPA system (3 min/image) with a single-element system (30 s/spectrum), it can be seen that if an area as small as $30 \mu\text{m} \times 30 \mu\text{m}$ were to be analyzed with a spatial discrimination of $10 \mu\text{m}$, the FPA-based system would have significant time advantages (3 min to at least 5 min). Thus, in terms of SNRs, the advantages of the single-element detector are quickly mitigated when a number of spectra are to be acquired. As a general rule, if a single spectrum of a sample is to be acquired, the single-element spectrometer is better suited given the cost of instrumentation. If a spatial area larger than tens of micrometers on the side to be examined, then an FPA-based

(30) Messerschmidt, R. G. Minimizing Optical Nonlinearities in Infrared Microspectroscopy. In *Practical Guide to Infrared Microspectroscopy*; Humecki, H. J., Ed.; Marcel Dekker: New York, 1995.

system is more useful. It is anticipated that improvements in FPA technology will only increase the advantages afforded by imaging spectrometers.

G. Developmental Directions for FPAs. Efforts to achieve higher data acquisition efficiency have been moderately successful through changes in the methodology of data collection. We believe, however, that major improvements in acquisition efficiency are difficult to achieve without changing the detector technology involved. Two changes incorporated into some FPA detectors available today (for example, a 256×256 element MCT) should allow this to occur. First, the integration time per frame must be increased to allow a corresponding increase in the acquisition ratio. The maximum integration time per frame would ultimately be limited by the dynamic range of the ADC. Second, high speed and multiple readout channels should provide a multiplex advantage in data readout. For example, the fastest frame rate of a dual-channel readout of a 256×256 element MCT is only one-third as slow as the fastest frame rate of a 16 times smaller array (64×64 element MCT) employing single-channel electronics. Ultimately, a situation can be visualized where a large number of digitization circuits and readout channels are present (to a limit of one per pixel). Improved detector fabrication would also contribute to more sensitive and accurate detectors. Once such hardware advances have been implemented, FPA imaging systems would be able to obtain high SNR, spatially resolved data in the same time as required for data collection of a single spectrum using a single detector in a conventional FT-IR spectrometer.

CONCLUSIONS

In presenting a systematic analysis of the data collection process in microimaging spectrometers, we derive an expression for the SNR in terms of the collection parameters. The effects of frame coaddition, image coaddition, spectral resolution, spatial homogeneity, FPA noise, interferometer characteristics, and computational processes are explicitly incorporated to achieve an understanding of the relationships between these variables. The predicted trends are observed experimentally, and the divergence for some cases is explained by an analysis of the FPA noise. Collection strategies are analyzed, and a method is suggested for obtaining optimal experimental conditions to obtain the highest possible SNR data in a given experimental time period. The theoretically predicted SNR was found to agree well with experimentally obtained values, and the SNR of data obtained from a single pixel was comparable to data obtained from a conventional single-element mapping spectrometer. Further, we describe a new data acquisition approach to improve the quality of acquired data. The theory developed in this paper should both provide useful guidelines in the design of experiments for this emerging technique and aid in better understanding of the various technological details required for improved FT-IR spectroscopic imaging applications.

Received for review April 3, 2001. Accepted August 13, 2001.

AC010380M